A Two-Color Beamline for Electron Spectroscopies at Diamond Light Source

Tien-Lin Lee & David A. Duncan

A Two-Color Beamline for Electron Spectroscopies at Diamond Light Source

TIEN-LIN LEE AND DAVID A. DUNCAN

Diamond Light Source Ltd., Didcot, Oxfordshire, UK

Diamond Light Source's Surface and Interface Structural Analysis beamline (I09) is the first in the world designed to deliver both hard and soft X-rays with optimized, independent sources and optics. With the extended energy range, we offer a wide variety of X-ray techniques that are based primarily on X-ray photoelectron and absorption spectroscopies, which can be combined to maximize the information one can extract from a visit to the beamline. For photoelectron spectroscopy, this energy range corresponds to an information depth from 0.5 to more than 20 nm, providing the bulk as well as surface sensitivity for depth-profiling of heterostructures and buried interfaces.

This unique combination has allowed I09 to develop, since becoming operational in 2013, a user community that is interested in two interconnected research areas. One concentrates on surface chemistry and structures, in particular adsorption of organic molecules on solid surfaces and epitaxial growth of two-dimensional materials. The other area of research deals with the electronic structures of oxide hetero-interfaces, electron correlations and metal-insulator transitions, energy research, functionalized materials, and material design. The vast majority of these studies, particularly those on surface structures and lithium ion batteries, have benefited from the use of both soft and hard X-rays at I09. In the following sections, we outline the design, science cases, and future plans of the beamline.

The I09 beamline

Figure 1 shows a schematic layout of the beamline, which is split into three branches: Branch I delivers hard X-rays and J and K soft X-rays. Branches I and J merge in Experimental Hutch 2 (EH2) to allow combined hard and soft X-ray experiments. Additional end-stations are being set up in Experimental Hutch 1 (EH1) and Experimental Cabin (EC) for hard and soft X-ray-only studies, respectively. With totally independent sources and optics, one soft and one hard X-ray experiment can be performed in parallel on two of the three stations.
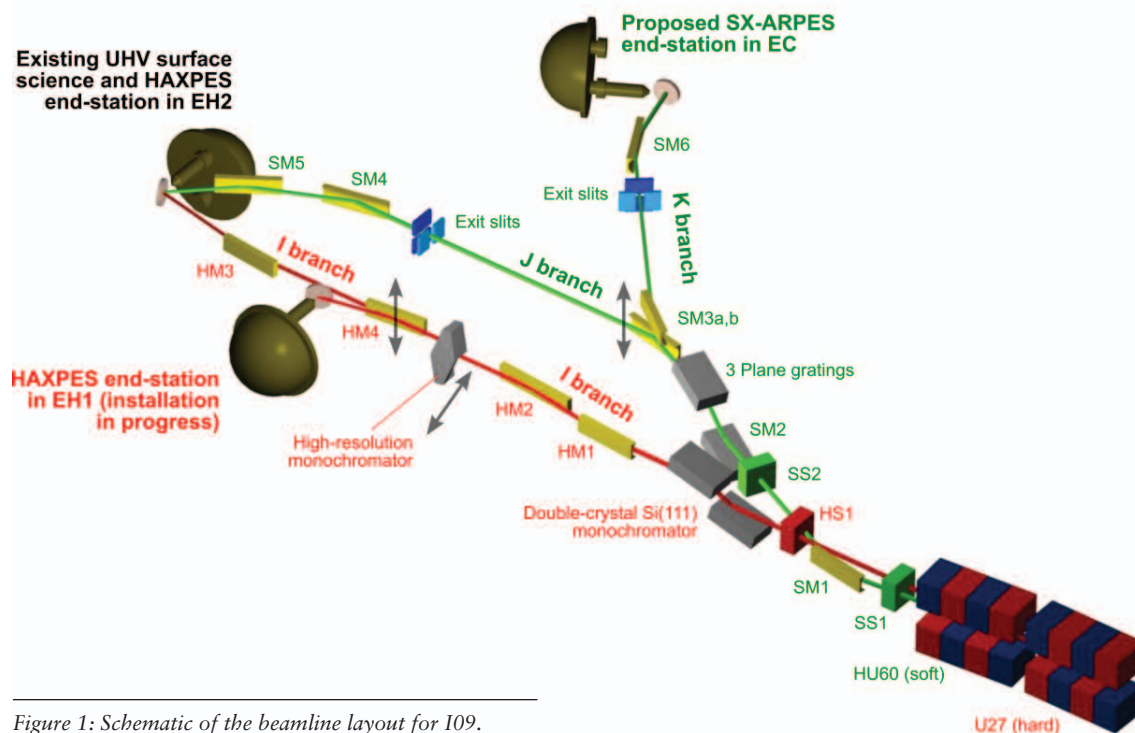

Figure 1: Schematic of the beamline layout for I09.

The beamline uses one of the four 8 m straight sections in the Diamond storage ring. To allow the hard X-ray undulator to reach a suitably small gap, additional magnets were added to create two minima in the vertical β function (β_y) over the straight section. Hard X-rays are delivered by a 2 m in-vacuum undulator with a magnetic period of 27 mm and a minimum gap of 5.2 mm. Its first and third harmonics start at approximately 0.9 and 2.4 keV. The soft X-ray undulator is a 2.3 m modified APPLE II device, with a magnetic period of 60 mm. The lowest energies accessible for the linear horizontal, circular, and linear vertical lights are about 100, 150, and 200 eV, respectively. The hard and soft undulators are canted by 1.3 mrad and each centered with one of the β_y minima.

The energy of the hard X-rays is selected by an in-house-developed Si(111) double-crystal monochromator (DCM) designed to work between 2.1 and 20+ keV. After the DCM, the beam is reflected horizontally by the first and second hard X-ray mirrors (HM1 and HM2, respectively) in optics hutch 1 (OH1). Two of the HM1 mirror optics focus the hard X-rays vertically to the end-station in EH2 for energies below and above 5 keV. HM2 has a flat mirror that keeps the exit beam of HM2 parallel to the incident beam of HM1. After entering EH2, the hard X-ray beam is focused horizontally to the sample by a third mirror, HM3. For HAXPES experiments, three Si channel-cut crystals, oriented to excite the (004), (333), and (202)/(404) reflections at 5.94, 5.95, and 4.07/8.14 keV, respectively, can be inserted in the beam in EH1 to improve the energy resolution. The design of the soft X-ray branches is based on the well-established concept of a plane grating monochromator (PGM) using a collimated light. Before the PGM, soft X-ray mirror 1 (SM1) collimates vertically and focuses horizontally the synchrotron lights. After the PGM, SM3 focuses the beam vertically to the exit slit of either Branch J or K. After the exit slit, SM4 and SM5 (SM6) refocus the beam to the end-station in EH2 (EC). The beamline optics and diagnostics allow a quick alignment of the focused X-rays of Branches I and J to the focal spot of the electron analyzer in EH2.

The experimental station in EH2, which became operational in mid-2013, consists of an analysis chamber and two sample preparation chambers. The analysis chamber is equipped with a Scienta EW4000 high-voltage electron analyzer, a nano-amp low-energy electron diffraction (LEED) optic, and a monochromatic vacuum ultraviolet light source. The preparation chambers, each fitted with a standard LEED optic, allow ion sputtering, sample heating (up to 1500°C), gas dosing, and physical vapor deposition for *in-situ* surface preparation. A large manipulator that positions the sample and provides polar and azimuth rotations is used for X-ray measurements at temperatures between 60 and 900 K. For samples prepared in users' home laboratories, two types of in-house-designed "suitcases" have been routinely used for sample transfer in an inert gas or static vacuum and in UHV. Users are encouraged to discuss technical developments or additional support they need with the beamline staffs to meet their experimental requirements.

To make the best use of the wide energy range available on I09, we offer a range of X-ray techniques to the user community. Normal incidence X-ray standing waves (NIXSW) and energy-scanned pho-toelectron diffraction (PhD) are employed to determine surface adsorbate structures. X-ray photoelectron spectroscopy (XPS) provides chemical information and can be exploited with either soft (SXPS) or hard X-rays (HAXPES) to vary the surface/bulk sensitivity. Resonant photoelectron spectroscopy (ResPES) is a powerful technique for enhancing weak contributions to valence band photoemission from buried or dilute systems with element specificity. X-ray absorption spectroscopy (XAS), currently available in total electron yield and Auger yield modes, probes the unoccupied states and is sensitive to orbital orientation, oxidation state, and hybridization. For studying momentum-resolved electronic structures, angle-resolved photoelectron spectroscopy (ARPES) has been performed on I09 with a He lamp, and technical development is underway to expand its applications to soft and hard X-ray ranges. The use of these techniques on I09 offers unique combinations for studying a wide range of materials, which will be highlighted in the following case studies.

Single-atom catalysis on magnetite (001) surface

There is a trend within modern catalysis research to increasingly rely upon the use of density functional theory (DFT) to develop an understanding of long-observed trends in reactivity and unravel complex reaction mechanisms. Efforts to screen, and even predict catalysts from first principles, are supported by rapid advances in computing power. However, the dramatic increase in the availability of computationally cheap functionals with which to run DFT calculations has resulted in a significant variation, functional to functional, in predicted adsorption energies. This variation in adsorption energy can result in the predicted temperature required to run a catalytic reaction to vary by over a hundred degrees. Thus, stringent experimental benchmarks are of the utmost importance in screening these DFT variants.

In collaboration with the Parkinson group at the Technical University of Vienna and the Payne group at Imperial College London, we have been studying the adsorption of metal adatoms and molecular species on the (001) surface of magnetite (Fe_3O_4). In work recently published in *Nanoscale* [1], we used the normal incidence X-ray standing wave (NIXSW) technique to precisely determine the three-dimensional geometry of Ag and Cu adatoms on Fe_3O_4(001) (Fig. 2a–c). Our results show that both adatoms occupy bulk-continuation cation sites, but with a markedly different height above the surface (0.43 ± 0.03 Å (Cu) and 0.96 ± 0.03 Å (Ag)) (Fig. 2d). DFT calculations using the Heyd–Scuseria–Ernzerhof (HSE) functional reproduce the geometry well, but the more common Perdew–Burke–Ernzerhof + U (PBE + U) and PBEsol + U approaches perform poorly.

Graphene on silicon carbide

The discovery of graphene has invigorated research in the field of surface science. There has been considerable investigation into modifying graphene's electronic properties for device applications through substituting the carbon atoms by other elements. Nitrogen is one of the most studied dopants for graphene, and the use of nitrogen-doped graphene-based components in, e.g., fuel cells and lithium-ion batteries has
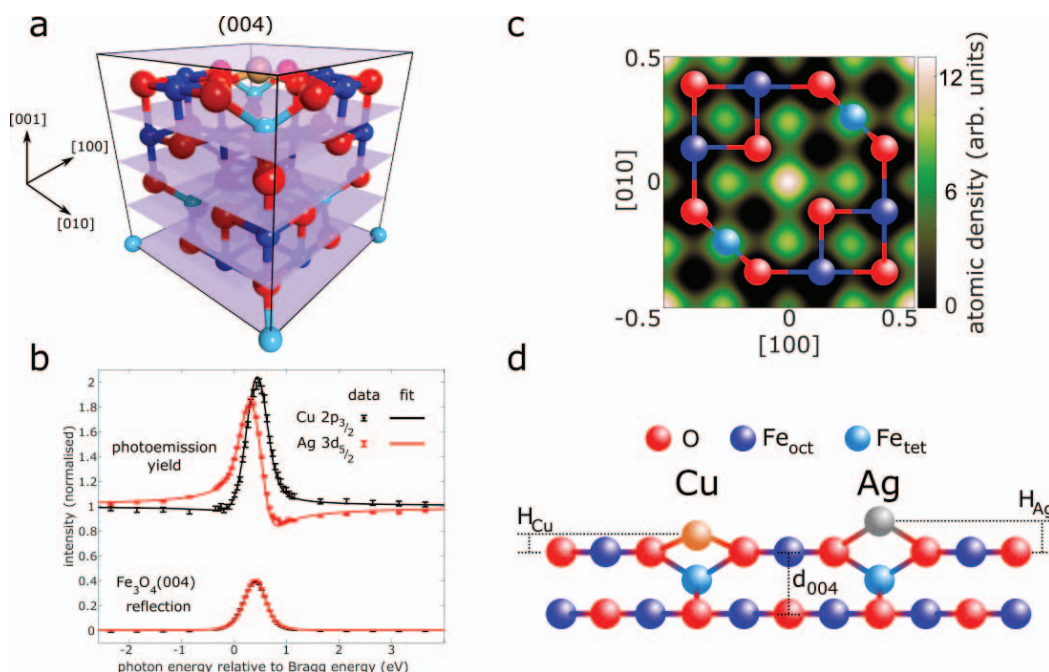
Figure 2: (a) $Fe_3O_4(001)$ surface with an adatom in the determined tetrahedral site and the (004) Bragg planes indicated, for which (b) the NIXSW profiles are shown for Cu and Ag adataoms. (c) Model-free 2D atomic density map of Cu adatoms on the $Fe_3O_4(001)$ surface reconstructed from Fourier analysis of three NIXSW measurements overlaid with the atomic structure of the $Fe_3O_4(001)$ surface; (d) to-scale schematic of the measured heights (H_{ad}) with respect to a bulk-like terminated $Fe_3O_4(001)$ surface [1].

demonstrated remarkable performance improvements. Yet our understanding of the doping process at the atomic level is still in its infancy.

To address this issue, Sforzini et al. [2, 3] probed the geometric structure of graphene on silicon carbide (SiC), with and without hydrogen intercalation, and before and after doping of nitrogen by sputtering. With the chemical sensitivity of XPS and the spatial resolution of NIXSW, multiple nitrogen species were identified; specifically, nitrogen doped into the graphene layer, doped into the SiC lattice, and

substituting the hydrogen intercalant (Fig. 3a). The nitrogen doping of an epitaxially grown monolayer of graphene (EMLG) resulted in little difference in the adsorption height of the graphene layer. However, the similar doping on hydrogen intercalated graphene (QFMLG) led to a significant increase in adsorption height (~0.3 Å), as well as an increase in the buckling of the layer (Fig. 3b).

Complementary ARPES measurements (Fig. 3c) indicated that hydrogen intercalated graphene contained fewer nitrogen dopants com-
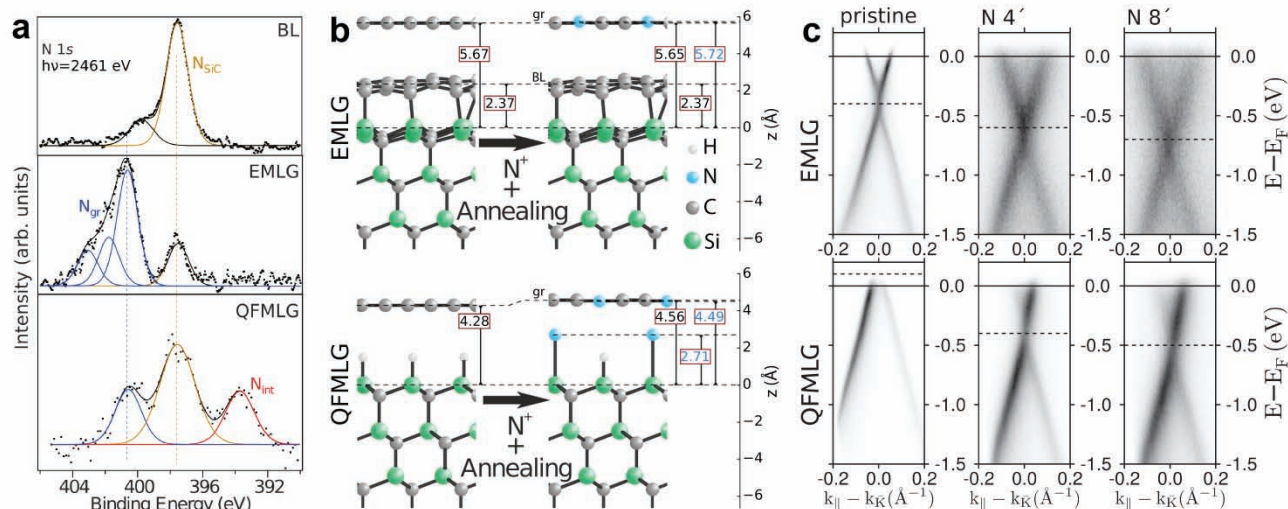

Figure 3: (a) N 1s XPS spectra for N-doped SiC terminated with a carbon buffer layer (BL), with an epitaxial grown monolayer of graphene (EMLG), and with a hydrogen intercalated quasi-freestanding monolayer of graphene(QFMLG); (b) summary of the vertical positions (in Å) measured by NIXSW for C, Si, and N in EMLG and in QFMLG, before and after N doping; (c) He Iα ARPES spectra of EMLG and QFMLG around the K point along the ΓK direction for pristine samples and those after 4 min and 8 min N doping [2, 3].
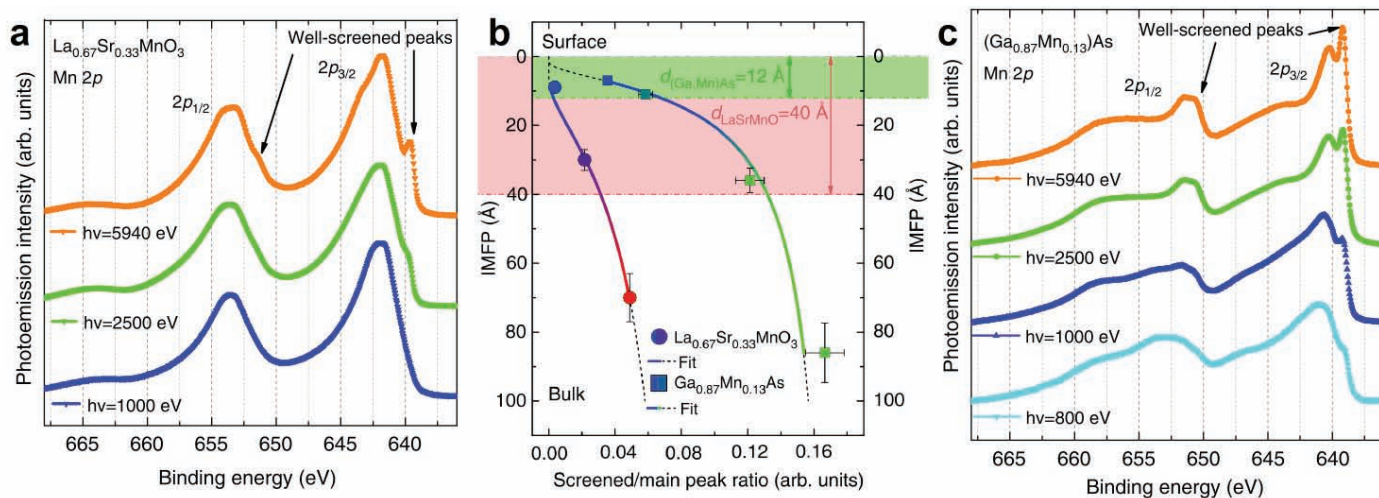
Figure 4: (a), (c) Mn 2p core level spectra recorded at various photon energies. The satellite on the low binding energy side of the main peak arises from screening of the 2p core holes by delocalized electrons. (b) Evaluation of the critical thicknesses of the surface transition layers for LSMO and (Ga,Mn)As based on the Mn 2p satellite-to-main-peak ratios versus the inelastic mean free path (which varies with the photon energy) [4].

pared to graphene without intercalation. However, this lack of dopants was compensated for by the proximity of nitrogen atoms substituting hydrogen at the interface that yield a similar number of charge carriers in graphene. This study presents clear evidence that, in terms of utilizing dopants to alter the electronic structure of graphene, the nature of the underlying support plays a vital role.

Critical thickness of electron hybridization in spintronics materials

Reduced dimensionality and translational symmetry can severely alter the electronic and magnetic properties of a spintronic material near the surface or an interface. In device applications, such modification can have a direct impact on the material's functionalities. In a study published in *Nature Communications*, Pincelli et al. [4] combined hard and soft X-ray photoelectron spectroscopies to verify the existence of such transition layers and to determine their thicknesses for thin films of dilute magnetic semiconductor (Ga,Mn)As and colossal magnetoresistive manganite $La_{1-x}Sr_xMnO_3$ (LSMO).

When a Mn 2p electron is ionized in a photoemission process, it is known that the core hole left behind may be screened by delocalized electrons, leading to a satellite on the lower binding energy side of the main peak in the core level spectrum, which reflects the strength of the 3d-ligand hybridization and the metallicity of the system.

Mn 2p spectra measured at I09 with photon energies between 800 eV and 6 keV, corresponding to an information depth approximately from 2 to 11 nm, revealed monotonically increasing intensity ratios and varying energy separations between the satellite and the main peak for (Ga,Mn)As and LSMO (Fig. 4a and c), which is well reproduced by theoretical calculations with the hybridization strength being the only varying parameter. A quantitative analysis of the attenuation of the satellites versus photon energy determined the critical thickness of

electron hybridization to be 1 and 4 nm for (Ga,Mn)As and LSMO, respectively (Fig. 4b). Such a crossover from surface to bulk metallicity is expected to be generic for spintronic materials and set lower limits on their dimensionalities for device applications.

Further measurements at SPring-8 using circularly polarized hard X-rays revealed clear magnetic circular dichroism (MCD) in the Mn 2p core levels for the two materials below their Curie temperatures, with the strongest magnetic contrast occurring at the satellites, confirming the major role of delocalized electrons in establishing the ferromagnetic coupling. It is envisaged that such MCD-in-HAXPES experiments will open up the possibility for assessing the interplay between metallicity and ferromagnetism as functions of temperature and depth in spintronic materials.

Battery materials

Li-ion batteries used in our daily life contain layered transition metal oxides as electrode materials. The layered structures facilitate migration of the Li ions in and out of the electrodes during charge and discharge processes. The multi-valence of transition metals allows the cations to self-adjust their oxidation states to maintain charge neutrality when lithiation or delithiation occurs. The effectiveness of Li ion intercalation, which is at the heart of the rechargeable battery performance, can therefore be evaluated by monitoring the oxidation states of the cations in the electrodes, which are directly accessible via X-ray photoelectron and absorption spectroscopies.

Vanadyl phosphate (ϵ-VOPO$_4$) is a promising cathode material that can potentially be intercalated with up to two Li$^+$ per vanadium. However, a full two Li$^+$ intercalation has not yet been demonstrated. In an electrochemical cycle, the intercalation of ϵ-VOPO$_4$ with the first Li$^+$ occurs between 3.5 and 4.5 V and the second one between 1.5 and 3.5 V (Fig. 5a). Previous work [5] has shown that the second Li$^+$ intercala-
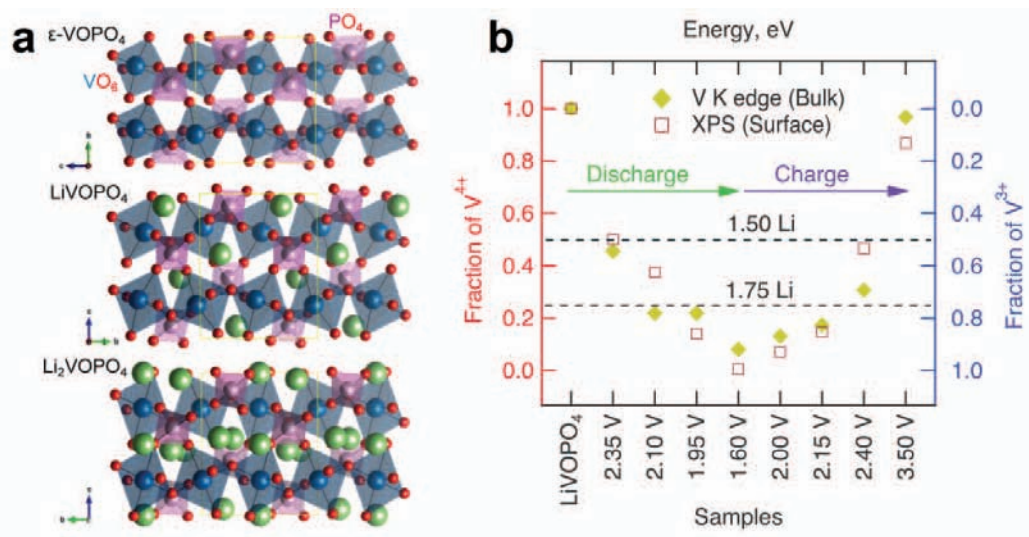
Figure 5: (a) Crystal structures of ε-VOPO$_4$ and corresponding lithiated LiVOPO$_4$ and Li$_2$VO-PO$_4$ phases [5]. (b) Comparison of V^{4+} contents determined by XPS (surface sensitive) and V K-edge XAS in transmission mode (bulk sensitive) indicates a uniform second Li ion intercalation throughout the low voltage window. Reproduced from [6] with the permission of AIP Publishing.

tion begins before the full incorporation of the first Li$^+$, resulting in a pronounced lithium gradient within the cathode, with the desirable Li$_2$VOPO$_4$ phase forming only near the surface.

In a study published in *Applied Physics Letters,* Wangoh et al. [6] aimed to establish that the intercalation of the second Li$^+$ can be ho-mogeneous if the intercalation of the first Li$^+$ is complete. They syn-thesized solid-state LiVOPO$_4$ electrodes (where the first interaction is complete) and cycled them within the low voltage window (1.5–3.5 V). The homogeneity of the Li$^+$ depth distribution was verified by compar-ing the V^{3+}/V^{4+} ratios measured from V 2p core level (surface sensi-
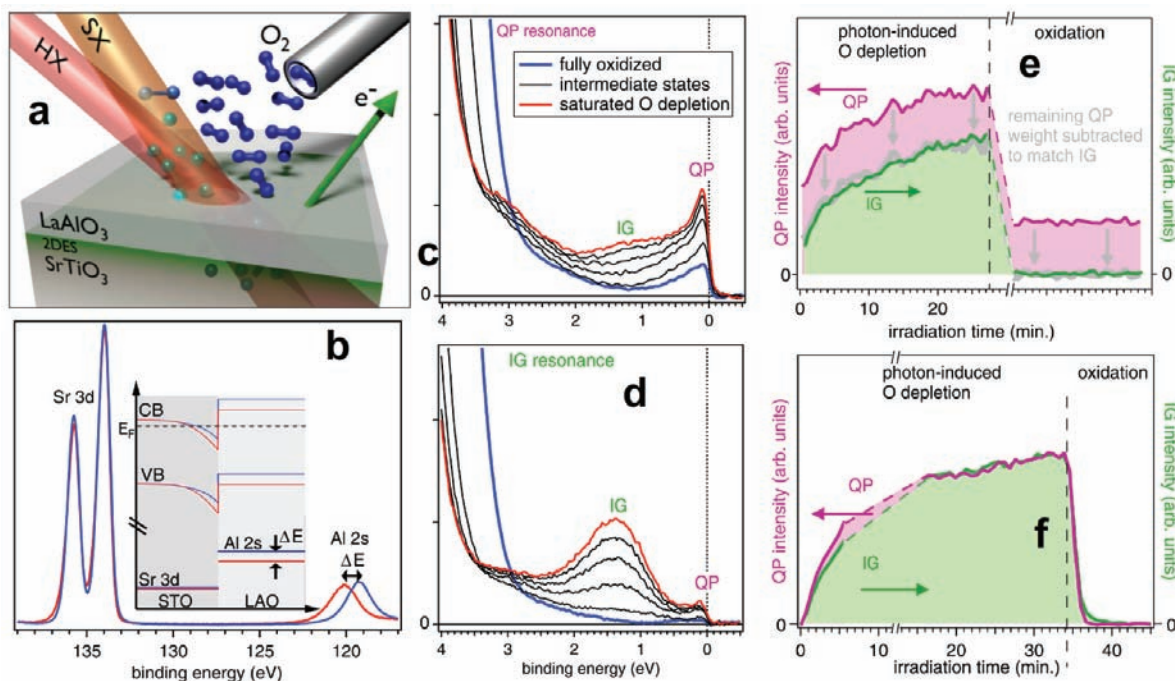

Figure 6: (a) Schematic of the experimental setup, where the samples are probed by either soft or hard X-rays that are intense enough to remove oxygen from the STO near the interface. Such oxygen loss can be counteracted by dosing of molecular oxygen via a capillary during an XPS measurement. (b) Sr 3d and Al 2s HAXPES spectra recorded with the interface in the full oxidation (blue) and the maximal O-depletion (red) states. The inset shows the corresponding alignments of the conduction band, valence band, and core levels across the interface. (c), (d) Valence-band spectra measured at the Ti L resonances maximizing the QP (c) and IG (d) intensity of a 4-unit-cell-thick LAO film grown on Nb:STO(001), where the interface is O-depleted to various extents. (e), (f) Comparison between the spectral weights of the QP and IG states for the 4 uc LAO/STO (e) and a bare STO surface (f) as oxygen vacancies are created by radiation exposure and eliminated by oxygen dosing [7].

tive) and from V K-edge XAS in transmission mode (bulk sensitive). As shown in Fig. 5b, the two ratios are very similar over the voltage range, indicating a uniform second Li$^+$ intercalation. A direct comparison between the pre-edge features in the O K-edge XAS (not shown) and DFT calculations further confirms Li$_{1.5}$VOPO$_4$ and Li$_{1.75}$VOPO$_4$ as two intermediate phases, which only form with uniform Li+ insertion. This study shows that it is the Li$^+$ incorporation kinetics in the high voltage regime that need to be improved to achieve the full two Li$^+$ capacity of ε-VOPO$_4$.

Two-dimensional electron systems at oxide-buried interfaces

It has been recently demonstrated that when band insulator LaAlO$_3$ (LAO) is grown epitaxially on another band insulator SrTiO$_3$ (STO), the buried interface turns conducting above a critical thickness of about four unit cells. Although the discovery of this two-dimensional electron gas (2DEG) has raised enormous interest in synthesizing a wide range of metal oxide heterostructures for novel electronic properties, the origin of the 2DEG is still under debate.

Among the various sources that have been put forward for the 2DEG, the two main contenders are oxygen vacancies and polar discontinuity. The former can result from an oxygen-depletion growth condition or radiation exposure. The idea of polar discontinuity is that, because Ti is 4+ while Al is 3+, in order to maintain local charge neutrality across the interface, it is necessary to transfer half an electron per unit cell from the LAO surface to the TiO$_2$ layer at the interface. In a study published in *Physical Review B*, Gabel et al. [7] showed how resonant photoelectron spectroscopy at the Ti L-edge can be used to disentangle these two contributions of mobile electrons.

Figure 6a depicts the experimental arrangement, where oxygen in STO can be effectively removed by synchrotron radiation and restored via *in-situ* molecular oxygen dosing. Figure 6b shows that the beam-induced oxygen depletion is concomitant with a stronger band bending across the interface, which is evident from a constant binding energy shift of all LAO core levels detected by HAXPES. The formation of each oxygen vacancy in STO releases two electrons—one is trapped in a defect state (binding energy ~ 1.3 eV) in the band gap and thus stays localized, while the other becomes delocalized and contributes to the 2DEG with a zero binding energy. They are often referred to as the in-gap (IG) and quasiparticle (QP) peaks, respectively. Figures 6c and d present the valence-band spectra of a 4-unit-cell-thick LAO film grown on Nb:STO(001) measured, with oxygen depleted to various degrees, at the Ti L resonances that maximize the QP (c) and IG (d) intensity. Figure 6e compares how the spectral weights of the QP and IG states for the LAO/STO evolve as oxygen vacancies in STO are created by radiation exposure and eliminated by oxygen dosing. It shows that they scale perfectly with each other, except for a constant offset in the QP intensity, which persists even when the IG state is fully suppressed, indicating that there is a 2DEG component that does not originate from oxygen vacancies. Further investigation reveals that this QP intensity offset completely vanishes for bare STO surfaces (Fig. 6f) and LAO/

STO interfaces where the LAO layers are either disordered or crystalline but thinner than four unit cells. Our findings therefore support the scenario that the remaining QP intensity which survives the oxygen dosing arises from polar discontinuity across the LAO/STO interface, and provide the first spectroscopic evidence for the existence of such an "intrinsic" 2DEG.

Metal-insulator transitions and electron correlations

Metal-insulator transitions (MITs) are widely observed in transition metal oxides and are closely linked to many exotic properties encountered in condensed matter physics. Modern theory predicts that an oxide with a narrow d or f band tends to turn insulating when the band is in the vicinity of being half-filled or the band width decreases. The evolution of the density of states from a normal metal, to a correlated metal, and to a Mott insulator is characterized by a continuous shift of the spectral weight from the Fermi level (often referred to as a QP) to the lower Hubbard band (LHB) until the QP vanishes and a band gap opens up. These spectral signatures can be directly observed by photoelectron spectroscopy.

There has been a long interest in vanadium dioxide in the condensed matter physics community due to the rich physics involved in its MIT.
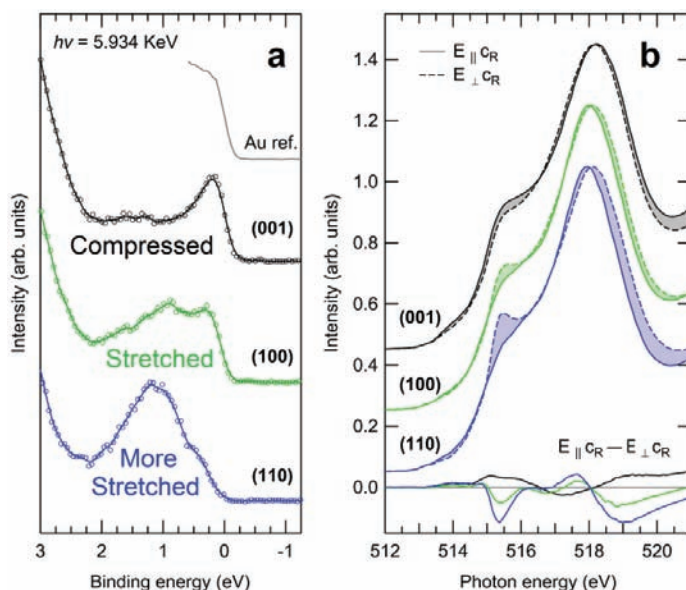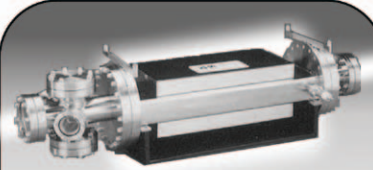

Figure 7: (a) Near Fermi-edge valence band spectra of VO$_2$ thin films grown on (001), (100), and (110) oriented TiO$_2$ substrates. All samples are measured 20 K above the respective rutile-to-monoclinic transition temperatures. As evidenced by the continuous shift of the spectral weight away from the Fermi level towards higher binding energies when the c$_R$ axis is increasingly stretched by the epitaxial strain, VO$_2$ behaves more and more like a Mott insulator that is observed for unstrained VO$_2$ only below the transition temperature. (b) Polarization-dependent V L-edge XAS and the orbital dichroism (bottom) for the three films measured above the respective transition temperatures. The dichroism of the most stretched film [(110)] resembles that of unstrained VO$_2$ below the transition temperature [8].

A recent renewal of the interest focuses more on how strain can be applied to altering the transition. The complexity of the MIT of VO_2 arises from a concomitant structural transition from a metallic, rutile (R) phase above the transition temperature (T_{MIT}) to an insulating, monoclinic (M1) phase below the T_{MIT}. Therefore, Peierls as well as Mott physics play a role in the MIT here. More specifically, theory has shown that the electronic properties of VO_2 are largely dictated by the V-V interaction along the c_R axis.

In a study published in *Physical Review B*, Mukherjee et al. [8] explore the influence of strain on electron correlation in VO_2 thin films epitaxially grown on rutile TiO_2 of three terminations, which stretch the VO_2 c_R axis to different extents. Their theory predicts that stretching the c axis leads to (1) reduction of the bandwidth of the V-V σ band and (2) a preferential filling that brings the σ band closer to being half-filled, the two requisites for triggering a MIT. Figure 7a shows the valence band spectra of the VO_2 films measured with HAXPES at 20 K above the respective R-M1 transition temperatures, where the spectral weight shifts away from the Fermi level toward the LHB as the c_R axis is further stretched, a clear fingerprint of a MIT. In Fig. 7b, linear dichroism in O K-edge XAS provides evidence for the preferential filling of the

σ band at photon energies around 515.3 eV. In contrast to unstrained VO_2, where the MIT goes hand in hand with the structural transition and is thus more Peierls-like, this study demonstrates that epitaxial strain can drive a rutile VO_2 into a Mott insulator, independent of the structural transition.

Future plans

Looking ahead, installation of a new HAXPES end-station in EH1 is underway. It is designed to be more versatile than the end-station in EH2 in accommodating HAXPES experiments with different requirements, which we plan to meet with a pool of exchangeable sample manipulator feedthroughs, each optimized for, e.g., high-throughput screening, in-operando HAXPES of device samples, or hard X-ray ARPES. We expect this new facility to welcome its first users in 2019. Further down the line, a third end-station, dedicated for soft X-ray ARPES, is being planned to use Branch K in EC. It will feature a momentum microscope being developed in collaboration with the Schöenhense group at University of Mainz and the Claessen group at University of Würzburg. We envisage that these developments will allow I09 to offer the user community improved capacity and flexibility for HAXPES studies and new opportunities for investigating momentum-resolved electronic structures. We should also be able to make more efficient use of the soft and hard X-rays once all three experimental stations have become operational. ∎

References

1. M. Meier et al., *Nanoscale* **10**, 2226–2230 (2018). doi:10.1039/C7NR07319D.
2. J. Sforzini et al., *Physical Review Letters* **114**, 106804 (2015). doi:10.1103/PhysRevLett.114.106804.
3. J. Sforzini et al., *Physical Review Letters* **116**, 126805 (2016). doi:10.1103/PhysRevLett.116.126805.
4. T. Pincelli et al., *Nature Communications* **8**, 16501 (2017). doi:10.1038/ncomms16051.
5. N. F. Quackenbush et al., *Chemistry of Materials* **27**, 8211 (2015). doi:10.1021/acs.chemmater.5b02145.
6. L. W. Wangoh et al., *Applied Physics Letters* **109**, 053904 (2016). doi:10.1063/1.4960452.
7. J. Gabel et al., *Physical Review B* **95**, 195109 (2017). doi:10.1103/PhysRevB.95.195109.
8. S. Mukherjee et al., *Physical Review B* **93**, 241110 (2016). doi:10.1103/PhysRevB.93.241110.